Heliyon

Received:
17 August 2018
Revised:
20 September 2018
Accepted:
15 November 2018

Cite as: Siva S. Panda, Adel S. Girgis, Atish Prakash, Leena Khanna, Pankaj Khanna, ElSayed M. Shalaby, Nehmedo G. Fawzy, Subhash C. Jain. Protective effects of *Aporosa octandra* bark extract against D-galactose induced cognitive impairment and oxidative stress in mice. Heliyon 4 (2018) e00951. doi: 10.1016/j.heliyon.2018.e00951

Protective effects of *Aporosa octandra* bark extract against D-galactose induced cognitive impairment and oxidative stress in mice

Siva S. Panda [a,b,*], **Adel S. Girgis** [c], **Atish Prakash** [d], **Leena Khanna** [b,e], **Pankaj Khanna** [b,f], **ElSayed M. Shalaby** [g], **Nehmedo G. Fawzy** [c], **Subhash C. Jain** [b]

[a] *Department of Chemistry and Physics, Augusta University, Augusta, GA 30912, USA*

[b] *Department of Chemistry, University of Delhi, Delhi 110007, India*

[c] *Department of Pesticide Chemistry, National Research Centre, Dokki, Giza 12622, Egypt*

[d] *Division of Pediatric CNS Infectious Diseases, Johns Hopkins University School of Medicine, Baltimore, MD 21205, USA*

[e] *Guru Gobind Singh Indraprastha University, Sector-16 C, Dwarka, New Delhi 110078, India*

[f] *Acharya Narendra Dev College, University of Delhi, Govindpuri, Kalkaji, New Delhi 110019, India*

[g] *X-Ray Crystallography. Lab., Physics Division, National Research Centre, Dokki, Giza 12622, Egypt*

[*] Corresponding author.

E-mail addresses: sspanda12@gmail.com, sipanda@augusta.edu (S.S. Panda).

Abstract

Aporosa octandra (Buch.-Ham. ex D.Don) Vickery is a native species of India. Different parts of the plant are used for the medicinal purpose by the tribal peoples of south-eastern part of India. However, the biological properties of *A. octandra* have not been studied well. The extracts obtained from the bark of *A. octandra* were evaluated to determine their protective effect on cognitive impairment and oxidative stress in mice induced by D-galactose using the standard protocol. Different dosages of extract **AOE-4** (100, 200, and 300 mg/kg, p.o.) were administered to mice, which were previously treated for six weeks with D-galactose (100 mg/kg s.c.). The D-galactose-induced mice showed significantly impaired cognitive behavior, i.e., oxidative defense, compared to the

https://doi.org/10.1016/j.heliyon.2018.e00951

sham group. Six weeks of treatment with *A. octandra* extract **AOE-4** (100, 200 and 300 mg/kg, p.o.) considerably improved the cognitive behavior and oxidative impairment of mice compared to the control alone (D-galactose). For the phytochemical investigation, the bark of *A. octandra* was successively extracted with dichloromethane and methanol. The chemical constituents of *A. octandra* were isolated by multiple column chromatography and characterized by different spectral analyses. (*R*)-Coclaurine (**AO-5**), an alkaloid, was isolated along with two other compounds from the **AOE-4** extract; three more compounds were also isolated from the **AOE-1** extract of the bark of *A. octandra*. All the compounds were isolated for the first time from the bark of *A. octandra*, and their structures were established by detailed spectral studies. The structure of compound **AO-5** was also investigated and confirmed by X-ray diffraction and DFT studies. This study highlights the protective effect of *A. octandra* bark extract against D-galactose-induced biochemically dysfunction in mice. (*R*)-Coclaurine (**AO-5**) was isolated as one of the major components of *A. octandra* bark from **AOE-4** extract; this compound could be further evaluated for the development of new potential drug candidates.

Keywords: Neuroscience, Plant biology

1. Introduction

Aging is a multifarious natural process, linked with several biochemical and morphological variations in the biological system [1]. Aging not only challenges the increased vulnerability as well as homeostasis network to the cognition and locomotion but also to physical, mental or social activities. The decrease in the level of polyunsaturated fatty acid like arachidonic acid in membrane fatty acid leads to cognitive deficits in the animal. Oxidative stress is also considered as one of the factors for the root cause of aging [2]. Age-related behavioral changes in motor and cognitive functions are not limited to the presence of neurodegenerative diseases like Alzheimer or Parkinson disease [3]. At the same time, aging could lead to the development of age-related diseases, such as neurodegenerative diseases [4], diabetes [5], and cardiovascular disorders [6], which are life-threatening challenges to the human beings [7].

Medicinal plants have been used since ancient time to cure and prevent various diseases. Several natural compounds such as isoflavones, anthocyanins, and catechins isolated from plant sources act as a potent antioxidant against ROS (Reactive Oxygen Species) [8]. Antioxidants, especially natural antioxidants are recommended for the prevention of aging [9]. Many Chinese medicinal herbs are considered as one of the possible interventions for the development of anti-aging drugs [10, 11, 12].

https://doi.org/10.1016/j.heliyon.2018.e00951

D-Galactose induced animal models are widely accepted and commonly used for identifying as well as studying aging, related oxidative damage and memory impairment [13, 14]. The normal metabolism of D-galactose, which is a reducing sugar controlled by galactose-1-phosphate uridyltransferase and D-galactokinase in animals however excess consumption of D-galactose leads to neurotoxicity because of abnormality in metabolism [15]. The toxicity is because of accumulation of galactitol in the cell, which causes osmotic stress and formation of ROS [16]. Many reports suggest that the formation of advanced glycation end products (AGE) is due to the interaction between D-galactose with the free amino groups of proteins, which further activates the receptor for advanced glycation end products (RAGE). In another word, D-galactose is responsible for oxidative stress and cellular damage [17, 18, 19].

In this study, we utilized an unexplored traditional medicinal plant *Aporosa octandra* (Buch.-Ham. ex D. Don) that belongs to the family Euphorbiaceae, sub-family Phyllanthaceae which is shrub to tree, up to 15 m high and comprises of 50 species that are distributed throughout India, Nepal, China, Pakistan, Thailand, and Malaysia (Fig. 1). It is commonly known as "Chantal" in India and "Kalikath" in Nepal. This plant is enlisted as a medicinal plant and is used for centuries in the Ayurvedic system [20].

The plants of this genus are reported to possess various medicinal properties. Traditionally, a decoction of the *A. octandra* bark (5−15 ml, 3−5 times daily) is used orally for treating inflammation, peptic ulcer, and hypotension. The fruit pulp is used for curing pimples while leaves are used to dye clothes black. Although this plant is used for many years as a traditional medicinal plant yet its phytochemical investigation is not reported to date and also this plant has never been screened for any oxidative stress studies. Therefore, the present study considers the bioassay of the extracts of its bark to explore the effect of behavioral and oxidative damage on D-galactose induced animal model. We have also considered the phytochemical investigation of the extracts.

2. Materials & methods

2.1. General

Melting points were measured in a Fischer Johns apparatus and are uncorrected. IR spectra were recorded on a Perkin−Elmer Spectrophotometer using KBr pellets. ^{1}H and ^{13}C NMR spectra were generated on Bruker 300 Spectrometer in deuterated solvents with TMS as an internal standard. The mass spectra were taken on Jeol Spectrophotometer. Silica gel of 60−120 mesh from Merck used for column chromatography.

https://doi.org/10.1016/j.heliyon.2018.e00951

Fig. 1. *Aporosa octandra* plant.

2.2. Plant material

Dried bark of *A. octandra* was collected from Baliguda, Odisha, India and identified by a Scientist from Odisha Forest Development Corporation (OFDC), Bhubaneswar, India. The dried bark was grounded to a fine powder using a blender under aseptic conditions.

2.3. Extraction and isolation

Dried and finely powdered bark (500 g) was extracted with cold CH_2Cl_2, CH_2Cl_2/MeOH (1:1) and MeOH separately for several hours in succession using mechanical stirrer. The organic solvent was removed from the extracts separately under reduced pressure to obtain dry extracts dichloromethane soluble part (*Aporosa octandra* extract-1, **AOE-1**, 11.2 g), dichloromethane: methanol (50:50) soluble part (*Aporosa octandra* extract-2, **AOE-2**, 15.8 g), and methanol soluble part (*Aporosa octandra* extract-3, **AOE-3**, 7.6 g), respectively. **AOE-2** and **AOE-3** were combined based on TLC similarities and named as **AOE-4**. Extracts **AOE-1** and **AOE-4** were then further fractionated by column chromatography and compounds **AO-1** to **AO-6** were isolated. Based on preliminary α,α-diphenyl-β-picrylhydrazyl (DPPH) free

https://doi.org/10.1016/j.heliyon.2018.e00951

radical scavenging studies with respect to standard ascorbic acid, **AOE-4** was further considered for animal studies.

Pentyl docosanoate (AO-1). Low melting solid (12 mg) [21]. IR ν_{max} (KBr): 2916, 2849, 1734, 1472, 1216, 1176, 761 cm^{-1}. ^{1}H NMR (δ, $CDCl_3$, 300 MHz): 4.05 (t, 2H, J = 3.8 Hz, -O-CH_2-), 2.29 (t, 2H, J = 4.6 Hz, -CH_2-C=O-), 1.58 (m, 4H, -CH_2CH_2-C=O & -CH_2CH_2-O), 1.25 (m, 40H, 20x-CH_2), 0.87 (t, 6H, J = 6.8, 7.0 Hz, 2x-CH_3). Mass Spectral data, EIMS m/z (%): 410 (100, M^+), 340 (38), 339 (25), 323 (18), 295 (51), 280 (15), 174 (10), 130 (20), 127 (35), 115 (48), 87 (10), 71 (21), 70 (80).

Tetradecanoic acid (AO-2). White solid (15 mg), m.p. 54−56 °C (lit. m.p. 54−55 °C, [22]). IR ν_{max} (KBr): 2916, 2848, 1698, 1454, 1217, 772, 726 cm^{-1}. ^{1}H NMR(δ, $CDCl_3$, 300 MHz): 2.37 (t, 2H, J = 7.3 Hz), 1.61 (m, 2H), 1.25 (brs, 20H, 10x-CH_2-), 0.88 (t, 3H, -CH_3, J = 6.6 Hz). ^{13}C NMR (δ, $CDCl_3$, 75.5 MHz): 176.2 (C=O), 33.7, 31.8, 29.5, 29.3, 29.1, 28.7, 24.6, 22.4, 13.9. Mass Spectral data, EIMS m/z (%): 229 (100), 211 (56), 197 (25), 183 (31), 155 (19), 113 (29), 85 (41).

Stigmast-5-en-3β-ol (AO-3). Colorless needles (40 mg), m.p. 134−135 °C [lit. 136−137 °C, [23]). IR ν_{max} (KBr): 3550, 3090, 2965, 1639, 1463, 1378, 1058, 1025, 930, 880, 803 cm^{-1}. ^{1}H NMR (δ, $CDCl_3$, 300 MHz): 5.38 (t, 1H, J = 6.9 Hz, H-6), 3.42 (m, 1H, H-3α), 2.32−1.34 (m, 3H, -CH_2-, -CH), 0.99 (s, 3H, 19-CH_3), 0.89 (d, 3H, J = 6.3 Hz, 21-CH_3), 0.84 (t, 3H, J = 7.0 Hz, 29-CH_3), 0.80 (d, 6H, J = 7.0 Hz, 26-CH_3 & 27-CH_3), 0.68 (s, 3H, 18-CH_3). ^{13}C NMR (δ, $CDCl_3$, 75.5 MHz): 141.2 (C-5), 121.3 (C-6), 71.3 (C-3), 59.9, 56.5, 50.5, 42.4, 40.0, 39.6, 37.5, 36.5, 36.4, 35.8, 32.3, 32.0, 31.6, 29.3, 28.3, 28.0, 24.3, 24.1, 22.5, 22.2, 21.2, 19.4, 18.8, 12.0, 11.3. Mass spectral data, EIMS *m/z* (%): 414 (M^+, 57), 399 (M^+-CH_3, 12), 396 (M^+-H_2O, 12), 381 (M^+-H_2O-CH_3, 6), 329 (9), 303 (14), 273 (M^+-side chain, 19), 255 (12), 232 [M^+-side chain-(C-15, C-16 & C-17), (16)], 213 (12), 173 (8), 164 [232 − (C-11, C-12, C-13, C-14 & C-19), (18)], 145 (20), 133 (19), 107 (35), 95 (37), 81 (45).

Stigmast-5-en-3-O-β-D-galactopyranoside (AO-4). White crystalline solid (20 mg), m.p. 274-75 °C (lit. m.p. 275-77 °C, [24]). IR ν_{max} (KBr): 3401, 2933, 2870, 1655, 1462, 1369, 1256, 1166, 1072, 1022, 800, 622 cm^{-1}. ^{1}H NMR (δ, DMSO-d_6, 300 MHz): 5.33 (t, 1H, J = 6.9 Hz, H-6), 4.67 (d, 1H, J = 3.6 Hz, -CHOH), 4.60 (d, 1H, J = 3.0 Hz, -CHOH), 4.41 (d, 1H, J = 3.6 Hz, -CHOH), 4.34 (d, 1H, J = 7.5 Hz, H-1′), 3.87 (t, 1H, J = 3.4 Hz, -CHOH), 3.77−3.64 (m, 3H, 3x-CHOH), 3.56 (m, 1H, H-3α), 3.37−3.19 (m, 3H, -CH_2OH, -CHOH), 2.39−1.01 (m, 29H), 0.97 (s, 3H, 19-CH_3), 0.90 (d, 3H, J = 6.3 Hz, 21-CH_3), 0.85 (t, 3H, J = 6.8 Hz, 29-CH_3), 0.80 (d, 6H, J = 6.5 Hz, 26 & 27-CH_3), 0.68 (s, 3H, 18-CH_3). ^{13}C NMR (δ, DMSO-d_6, 75.5 MHz): 140.6 (C-5), 121.4 (C-6), 101.1 (C-1′), 77.4 (C-2′, C-3′, C-4′, C-5′), 77.0, 76.6, 73.7, 70.4 (C-3), 61.5 (C-6′), 56.5, 55.7, 49.9, 45.5, 42.1, 40.7, 39.6, 38.6, 37.1, 36.5, 35.7, 33.7, 31.7,

https://doi.org/10.1016/j.heliyon.2018.e00951

29.5, 29.0, 28.0, 25.8, 24.1, 22.9, 20.8, 19.9, 19.3, 19.1, 18.8, 12.0, 11.8. Mass spectral data, EIMS *m/z* (%): 414 (M^+-galactose,18), 396 (M^+-galactose-H_2O, 16), 381 (M^+-galactose-H_2O-CH_3, 6), 329 (9), 303 (10), 256 (M^+-galactose-$C_{10}H_{21}$, 15), 215 (M^+-galactose-$C_{10}H_{21}$-carbons of C-15, C-16 & C-17, 5), 180 (galactose, 12), 147 (215-carbons of C-11, C-12, C-13, C-14 & C-19, 18), 133 (19), 107 (35), 95 (37), 81 (45), 57 (50), 43 (100).

(R)-1-(4-hydroxybenzyl)-6-methoxy-1,2,3,4-tetrahydroisoquinolin-7-ol compound with hydrogen sulfide (1:1) hydrate (AO-5). Colorless crystalline solid (160 mg, obtained from ethanol through slow evaporation technique) having m.p. 258−259 °C. IR ν_{max} (KBr): 3483, 3257, 2925, 1608, 1522, 1447, 1375, 1260, 1206, 1122, 1031, 837, 804, 623 cm^{-1}. ^1H NMR (δ, MeOH-d_4, 300 MHz): 7.15 (d, 2H, $J = 8.4$ Hz), 6.79 (d, 2H, $J = 8.4$ Hz), 6.74 (s, 1H), 6.64 (s, 1H), 4.58 (t, 1H, $J = 9.2$ Hz), 3.84 (s, 3H, -OCH_3), 3.46 (m, 2H), 3.33 (m, 2H), 3.01 (m, 2H). ^{13}C NMR (δ, MeOH-d_4, 75.5 MHz): 158.1, 149.2, 146.7, 131.8, 126.9, 124.9, 123.7, 117.0, 114.1, 112.6, 57.9, 56.5, 41.0, 40.5, 26.0. Mass Spectral data, HRMS (+ESI-TOF) *m/z* for $C_{17}H_{19}NO_3$ $[M+1]^+$calcd. 286.1368, found 286.1375. Specific Rotation: $[\alpha]^{27} = +2.10$ (C: 0.01, Methanol).

β-D-Fructofuranosyl-α-D-glucopyranoside (AO-6). White crystaline solid (140 mg), m.p. 187−189 °C (lit. m.p. 186−188 °C, [25]). IR ν_{max} (KBr): 3390, 2938, 1639, 1461, 1438, 1346, 1324, 1280, 1239, 1209, 1131, 1068, 990, 941, 910, 866, 848, 683, 550 cm^{-1}. ^1H NMR (δ, D_2O, 300 MHz): 5.35 (d, 1H, $J = 3.6$ Hz, -CHOH), 4.16 (d, 1H, $J = 8.6$ Hz, -CHOH), 3.99 (t, 1H, $J = 6.6$ Hz, -CHOH), 3.84 (m, 2H, 2x-CHOH), 3.76 (m, 4H, 2x-CH_2OH), 3.69 (d, 1H, $J = 9.4$ Hz, -CHOH), 3.62 (s, 2H, -CH_2OH), 3.50 (m, 1H, -CHOH), 3.47 (t, 1H, $J = 9.2$ Hz, -CHOH). ^{13}C NMR (δ, D_2O, 75.5 MHz): 104.7, 93.1, 82.3, 77.5, 75.0, 73.6, 73.4, 72.0, 70.2, 63.3, 62.4, 61.1. Mass Spectral data, EIMS *m/z* (%): 324 (M^+-H_2O, 4), 310 (7), 181 (5), 166 (4), 148 (6), 126 (8), 114 (12), 108 (5), 102 (16), 96 (11), 84 (17), 72 (100), 60 (80), 57 (78), 43 (90).

2.3.1. Single crystal X-ray of AO-5

Oxford CCD diffraction equipped with an Xcalibur Sapphire device (graphite monochromatic Mo-Kα radiation, $\lambda = 0.71073$ Å) was used for X-ray single crystal diffraction studies collected at 120 K using. Multiscan absorption corrections [26]. Table 1 exhibits the data collected and refinement parameters. SUPERFLIP was used for solving the structure [27] implemented in *CRYSTALS* program suit [28]. The refinement was carried out by a full-matrix least-squares method on the positional and anisotropic temperature parameters of all non-hydrogen atoms based on F^2 using *CRYSTALS* package. Hydrogen atoms were located geometrically and refined [29]. General-purpose crystallographic tool *PLATON* was used for structure

https://doi.org/10.1016/j.heliyon.2018.e00951

investigation [30]. Molecular graphics were prepared by *ORTEP-3* for Windows and *MERCURY* [31, 32].

Supporting information (CIF files) can be obtained from the CCDC database (CCDC-1588571).

2.3.2. Computational studies

2.3.2.1. Structure optimization

Density functional theory (DFT, ground state, in-vacuo) was undertaken for molecular structure optimization for compound **AO-5** applying hybrid functional B3LYP (Becke's three-parameter hybrid functional) with 6-311G+(2d,p) basis set, utilizing the Gaussian 03 package (Tables 2 and 3, Fig. 2) [33].

2.3.2.2. Vibrational studies

Computed vibrational studies of compound **AO-5** were undertaken by Gaussian 03 software using the optimized geometry [DFT/B3LYP/6-31G(d) basis set]. To correct the theoretical errors, the scaled factor of 0.9594 was considered for all the IR

Table 1. Refinement details and crystal data of compound **AO-5**.

Parameter	Crystal data
Chemical formula	$C_{17}H_{23}NO_4S$
M_r	337.44
Crystal system, space group	Monoclinic, $P2_12_12$
Temperature (K)	293
a, b, c (Å)	7.1112 (3), 18.9612 (8), 12.5124 (6)
V (Å^3)	1687.13 (8)
Z	4
Radiation type	MoKα
Diffractometer	
T_{min}, T_{max}	0.639, 0.908
No. of measured, independent and observed [I > 2σ(I)] reflections	36592, 5886, 4900
R_{int}	0.03
$(\sin\theta/\lambda)_{max}$ (Å^{-1})	0.759
$R[F^2 > 2\sigma(F^2)]$, $wR(F^2)$, S	0.049, 0.113, 1.02
No. of reflections	4900
No. of parameters	209
$\Delta\rho_{max}$, $\Delta\rho_{min}$ (e Å^{-3})	0.46, −0.38

https://doi.org/10.1016/j.heliyon.2018.e00951

Table 2. Selected intramolecular experimental (X-ray) and computational optimized geometrical parameters (bond lengths, Å) of compound **AO-5**.

Geometric parameters	Experimental X-ray data	DFT
O2—C3	1.374	1.371
C3—C4	1.383	1.393
C3—C8	1.362	1.391
C4—C5	1.391	1.387
C5—C6	1.393	1.400
C6—C7	1.383	1.395
C6—C9	1.512	1.512
C7—C8	1.395	1.392
C9—C10	1.529	1.547
C10—N11	1.5	1.463
C10—C15	1.515	1.526
N11—C12	1.496	1.458
C12—C13	1.505	1.523
C13—C14	1.508	1.513
C14—C15	1.391	1.397
C14—C20	1.394	1.402
C15—C16	1.403	1.401
C16—C17	1.379	1.380
C17—O18	1.366	1.366
C17—C19	1.402	1.402
C19—C20	1.378	1.384
C19—O21	1.374	1.374
O21—C22	1.425	1.421
RMSE	—	0.015
Maximum difference	—	0.038

frequencies. Avogadro 1.1.1 software was used to simulate the spectra of **AO-5** [34] (Table 4).

2.3.2.3. NMR studies

Computed NMR studies of compound **AO-5** was carried out by Gaussian 03 program, DFT/B3LYP/6-311G+(2d,p)/GIAO (Gauge-Independent Atomic Orbital) for the optimized structure at the same level of theory. The predicted ^{1}H and ^{13}C NMR chemical shifts were derived from the equation; $\delta = (\text{intercept} - \sigma)/-\text{slope}$, where δ is the scaled chemical shift values (δ relative to TMS), σ is the computed

https://doi.org/10.1016/j.heliyon.2018.e00951

Table 3. Selected intramolecular experimental (X-ray) and computational optimized geometrical parameters (bond angles, °) of compound **AO-5**.

Geometric parameters	Experimental X-ray data	DFT
O2—C3—C4	121.2	117.53
O2—C3—C8	118.26	122.78
C4—C3—C8	120.52	119.69
C3—C4—C5	119.4	119.67
C4—C5—C6	121.08	121.78
C5—C6—C7	118.01	117.51
C5—C6—C9	120.76	120.93
C7—C6—C9	121.23	121.56
C6—C7—C8	121.1	121.47
C7—C8—C3	119.9	119.89
C6—C9—C10	113.56	113.49
C9—C10—N11	108.45	108.50
C9—C10—C15	115.13	112.93
N11—C10—C15	110.31	110.59
C10—N11—C12	112.49	113.53
N11—C12—C13	109.93	108.05
C12—C13—C14	112.65	110.78
C13—C14—C15	121.91	121.20
C13—C14—C20	118.42	119.29
C15—C14—C20	119.61	119.50
C10—C15—C14	121.17	121.32
C10—C15—C16	119.82	119.77
C14—C15—C16	118.78	118.85
C15—C16—C17	121.64	121.52
C16—C17—O18	124	119.91
C16—C17—C19	118.96	119.57
O18—C17—C19	117.02	120.52
C17—C19—C20	119.76	119.43
C17—C19—O21	115.77	114.40
C20—C19—O21	124.46	126.17
C14—C20—C19	121.18	121.12
C19—O21—C22	116.17	118.19
RMSE	—	1.66
Maximum difference	—	4.52

https://doi.org/10.1016/j.heliyon.2018.e00951

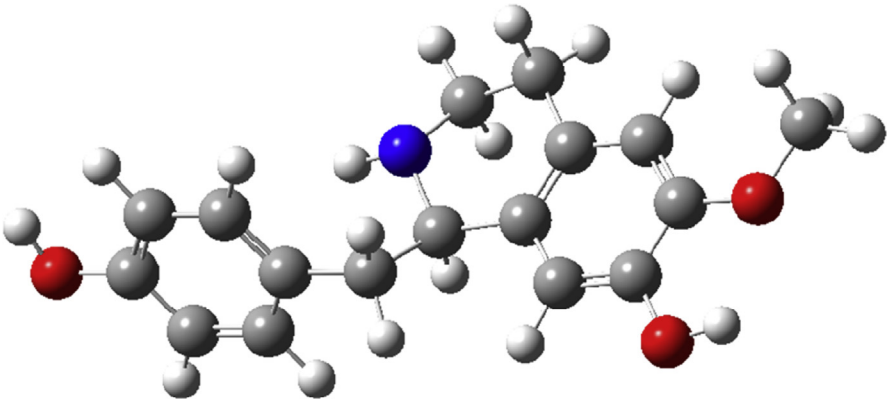

Fig. 2. A projection of the optimized structure of compound **AO-5** by DFT/B3LYP method with 6-311G+(2d,p) basis set.

isotropic shielding constants and the slope (for ^{1}H NMR = 1.0593, ^{13}C NMR = 1.0228) and intercept (for ^{1}H NMR = 32.0706, ^{13}C NMR = 181.3782) from the linear regression analysis [35], http://cheshirenmr.info/ScalingFactors.htm) (Table 5).

2.3.3. Biological studies

2.3.3.1. Animals

Male LACA 2−3 months old mice (25−30 g), (Central Animal House, Punjab University, India) were used. Prior to the experiment all the animals were acclimatized to the laboratory environment. A standard protocol approved by the Institutional Animal Ethics Committee followed in accordance with the Indian National Science Academy Guidelines to keep and care the animals in the facility. All the animal studies were carried out between 9.00 and 17.00 h.

2.3.3.2. Drugs and treatment schedule

D-galactose and optimized extract of *Aporosa octandra* (**AOE-4**) were used for the study. D-galactose made with deionized water for subcutaneous (s.c.) administration. **AOE-4** solution administered to the mice orally in a dose of 1 ml/100g body weight which was prepared by suspending AOE-4 in 0.25% w/v sodium carboxymethyl cellulose. Animals were randomized into eight groups, consists of 5 animals in each.

I. Naïve group administered 0.5% Sodium carboxymethyl cellulose.

II. D-galactose treated group administered 100 mg/kg of D-galactose subcutaneously.

https://doi.org/10.1016/j.heliyon.2018.e00951

Table 4. Calculated vibrational spectra (IR) of compound **AO-5**.

Scaled freq. (cm^{-1})	Intensity	Scaled freq. (cm^{-1})	Intensity	Scaled freq. (cm^{-1})	Intensity
79	0.72	882	13.14	1455	1.59
85	1.63	895	5.20	1471	18.84
126	0.88	898	5.36	1472	0.77
136	0.04	917	2.89	1473	0.76
154	0.27	923	12.90	1481	0.79
191	0.80	942	10.07	1484	3.10
213	0.35	970	1.38	1506	22.07
251	1.77	991	0.28	1531	9.29
289	0.67	1005	21.64	1537	11.76
302	2.55	1008	1.53	1592	52.33
307	0.13	1030	2.51	1612	1.91
339	3.92	1044	8.47	1630	68.06
360	2.91	1066	40.81	1646	94.24
365	73.94	1078	7.69	1787	18.60
374	7.07	1127	41.72	1794	5.05
386	2.34	1146	3.48	1817	4.14
399	58.57	1173	22.53	1824	29.11
404	2.79	1189	0.76	2694	36.99
415	5.01	1191	28.61	2741	52.63
429	0.47	1205	7.87	2757	16.50
447	0.73	1212	100.00	2773	41.32
466	1.18	1214	66.70	2783	18.85
497	3.99	1224	2.19	2789	39.21
520	6.27	1232	25.91	2794	35.81
535	5.41	1238	12.12	2812	14.21
566	2.32	1243	1.96	2838	28.17
600	5.50	1254	54.67	2842	21.17
612	8.54	1266	68.27	2898	26.44
644	0.48	1293	2.62	2907	8.81
650	1.26	1317	5.39	2925	23.87
658	1.21	1324	62.81	2927	17.87
719	2.70	1337	64.87	2928	0.45
759	0.89	1350	7.70	2933	4.74
793	2.86	1352	17.64	3005	0.36
826	54.31	1368	8.15	3580	60.48
852	23.52	1389	38.11	3581	26.36
867	9.21	1403	93.45		

https://doi.org/10.1016/j.heliyon.2018.e00951

Table 5. Theoretical ^{1}H and ^{13}C NMR chemical shifts (δ, ppm) of compound **AO-5**.

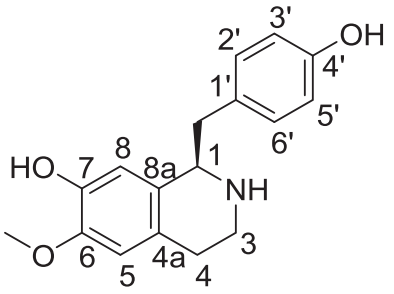

Atom	Calculated (δ, ppm) DFT/B3LYP method with 6-311G + (2d,p) basis set
NH	1.45
H_2C-4	2.84, 3.43 (average = 3.14)
Benzyl CH_2	2.76, 3.83 (average = 3.30)
H_2C-3	3.26, 3.50 (average = 3.38)
H-1	4.21
OCH_3	4.12, 4.14, 4.48 (average = 4.25)
OH	3.64
OH	4.71
H-5	6.24
H-3'/5′	6.19, 6.64 (average = 6.42)
H-8	6.68
H-2'/6′	6.93, 7.04 (average = 6.99)
H_2C-4	35.5
Benzyl CH_2	46.1
H_2C-3	48.8
OCH_3	55.0
HC-1	59.1
C-5	102.4
C-8	103.6
C-3′	104.6
C-5′	106.9
C-4a	116.8
C-2′	120.6
C-1′	122.6
C-8a	123.0
C-6′	124.6
C-7	135.9
C-6	137.0
C-4′	146.5

https://doi.org/10.1016/j.heliyon.2018.e00951

III, IV & V. **AOE-4** (100, 200 & 300 mg/kg p.o.) solution was administered to the per se groups.

VI, VII & VIII. **AOE-4** (100, 200 & 300 mg/kg, p.o.) was administered to D-galactose treated mice.

The study was carried out for a period of 42 days (6 weeks).

2.4. Behavioral assessments

2.4.1. Assessment of cognitive performance

2.4.1.1. Morris water maze experiment

The Morris water maze technique was used to evaluate the acquisition and retention of memory [13, 14]. Morris water maze is a large circular pool of 45 cm in height and 150 cm in diameter, filled with of water at 28 ± 1 °C to a depth of 30 cm. The pool was used to carry out the experiments by following the procedure described in the report [14].

2.4.1.2. Maze acquisition phase (training)

All the Animals trained with 4 trials in each session on day 20. Every trial was having different starting position. The time taken by the mouse to reach the visual platform was noted as the initial acquisition latency (IAL). After the end of each trial, mice were directed to their respective home cages.

2.4.1.3. Maze retention phase (testing for retention of the learned task)

On day 21 (following 24 hours) and 21 days (day 42) after IAL, the mice was released randomly at one of the edges facing the wall of the pool to assess for memory retention. Time taken by mice to find the hidden platform on day 21 and 42 following D-galactose administration were recorded, labeled as first retention latency (1^{st} RL) and second retention latency (2^{nd} RL) respectively.

2.4.2. Assessment of gross behavioral activity

Gross behavioral activity was observed at weekly interval. Each animal was placed in a square (30 cm) closed arena equipped with infrared light-sensitive photocells using digital actophotometer. The animal was observed for a period of 5 min and expressed as counts/5 min. The apparatus was placed in a darkened, light and sound attenuated and ventilated test room [13].

https://doi.org/10.1016/j.heliyon.2018.e00951

2.4.3. Biochemical assessment

Biochemical tests were conducted after performing the Morris water Maze task paradigm. The animals were sacrificed and brains were removed and rinsed with ice-cold isotonic saline. Brains were then homogenized with ice-cold 0.1 mmol/L phosphate buffer (pH 7.4). The homogenates (10 % w/v) were then centrifuged at 10,000 rpm for 15 min and the supernatant so formed was used for the biochemical estimations.

2.4.4. Measurement of lipid peroxidation

The quantitative measurement of lipid peroxidation in brain tissue was performed according to the method described by Wills, 1966 [36]. The amount of malondialdehyde (MDA), a marker of lipid peroxidation was assayed in the form of thiobarbituric acid reacting substances (TBARS). Briefly, 0.5 ml of supernatant containing 0.5 ml TrisHCl was incubated at 37 °C for 2 h. After incubation, 1 ml of 10 % trichloroacetic acid (TCA) was added and centrifuged at 10,000 rpm for 10 min and from the resulting supernatant 1 ml of it was collected which was further followed by the addition of 1ml of 0.67% thiobarbituric acid (TBA). Lastly, the tubes were kept in boiling water for 10 min. After cooling 1 ml double distilled water was added and absorbance was measured at 532 nm using a spectrophotometer (Shimadzu, Japan). TBARS were quantified using an extinction coefficient of 1.56×10^5 $M^{-1}cm^{-1}$ and expressed as nmol of MDA per mg protein [13].

2.4.5. Superoxide dismutase activity

Superoxide dismutase (SOD) activity was determined by following the reported method [37]. A mixture of 0.1 mM of EDTA, 50 mM of sodium carbonate and 96 mM of nitro blue tetrazolium (NBT) were used for the assay. 2 ml of the above mixture, 0.05 ml of hydroxylamine and 0.05 ml of the supernatant were mixed and then the auto-oxidation of hydroxylamine was measured for 2 min at 30 sec interval by at 560 nm using Perkin Elmer Lambda 20 spectrophotometer [13].

2.4.6. Estimation of acetylcholinesterase (AChE) activity

AChE is a marker of loss of cholinergic neurons in the brain region. The standard Ellman method was used to assess the AChE [38]. The Ellman reagent (0.1 ml) was missed with 0.05 ml of supernatant, 3 ml of sodium phosphate buffer (pH 8), and 0.1 ml of acetylthiocholine iodide and the change in absorbance was measured for 2 min at 30 s interval at 412 nm using Perkin Elmer Lambda 20 spectrophotometer. Results were expressed as micromoles of acetylthiocholine iodide hydrolyzed per min per mg of protein [13].

https://doi.org/10.1016/j.heliyon.2018.e00951

2.4.7. Protein estimation

The protein content was estimated by the Biuret method [39] using bovine serum albumin as a standard.

2.4.8. Statistical analysis

Values are expressed as mean ± SEM (standard error mean). The behavioral assessment data were examined by a repeated measures two-way analysis of variance (ANOVA) with treated groups as between and sessions as the within-subjects factors. The biochemical estimations were analyzed by one-way ANOVA and Post hoc comparisons between groups were made using Tukey's test. $P < 0.05$ was considered significant.

3. Results & discussion

3.1. Fractionation of AOE-1 and AOE-4 extracts

The column was packed with silica gel of 120 mesh size and eluted with a gradient of hexanes/CH_2Cl_2/MeOH. A total of 97 fractions (300 ml each) from **AOE-1** were collected and combined on the basis of their TLC behavior to make seven major fractions (F1−F7). Similarly, 95 fractions (300 ml each) were collected from **AOE-4** and pooled based on their TLC behavior to make nine major fractions (F1a−F9a). Isolation of the compounds was accomplished upon repeated column chromatography of fractions collected from **AOE-1** and **AOE-4** followed by crystallization. Three compounds, pentyl docosanoate (**AO-1**, 12 mg), tetradecanoic acid (**AO-2**, 15 mg) and stigmast-5-en-3β-ol (**AO-3**, 40 mg) were isolated from **AOE-1**. Similarly, stigmast-5-en-3-O-β-D-galactopyranoside (**AO-4**, 20 mg), **(*R*)-1-(4-**hydroxybenzyl)-6-methoxy-1,2,3,4-tetrahydroisoquinolin-7-ol ((*R*)-Coclaurine **AO-5**, 160 mg) and β-D-fructofuranosyl-α-D-glucopyranoside (**AO-6**, 140 mg) were isolated from **AOE-4**. All these compounds are reported here for the first time from *Aporosa octandra* (Figs. 3 and 4). All the isolated compounds were fully characterized by various spectroscopic techniques and confirmed with the reported data. Compound **AO-5** is an alkaloid also isolated earlier from the leaves of *Nelumbo nucifera* [40], the root and bark of *Xylopia parviflora* [41] and from the stems of *Aristolochia ridicula* [42]. Even the structure of (*R*)-Coclaurine was reported earlier, herein for the first time we investigated the structure by X-ray and DFT studies.

3.2. Single crystal X-ray studies

The crystal structure of compound **AO-5** was confirmed by single crystal X-ray diffraction studies. Compound **AO-5** crystallizes in the orthorhombic space group $P2_12_12$ with tetrahydroisoquinoline scaffold. It consists of a p-hydroxybenzyl moiety nearly perpendicular to the tetrahydroisoquinolinyl heterocycle with a dihedral

https://doi.org/10.1016/j.heliyon.2018.e00951

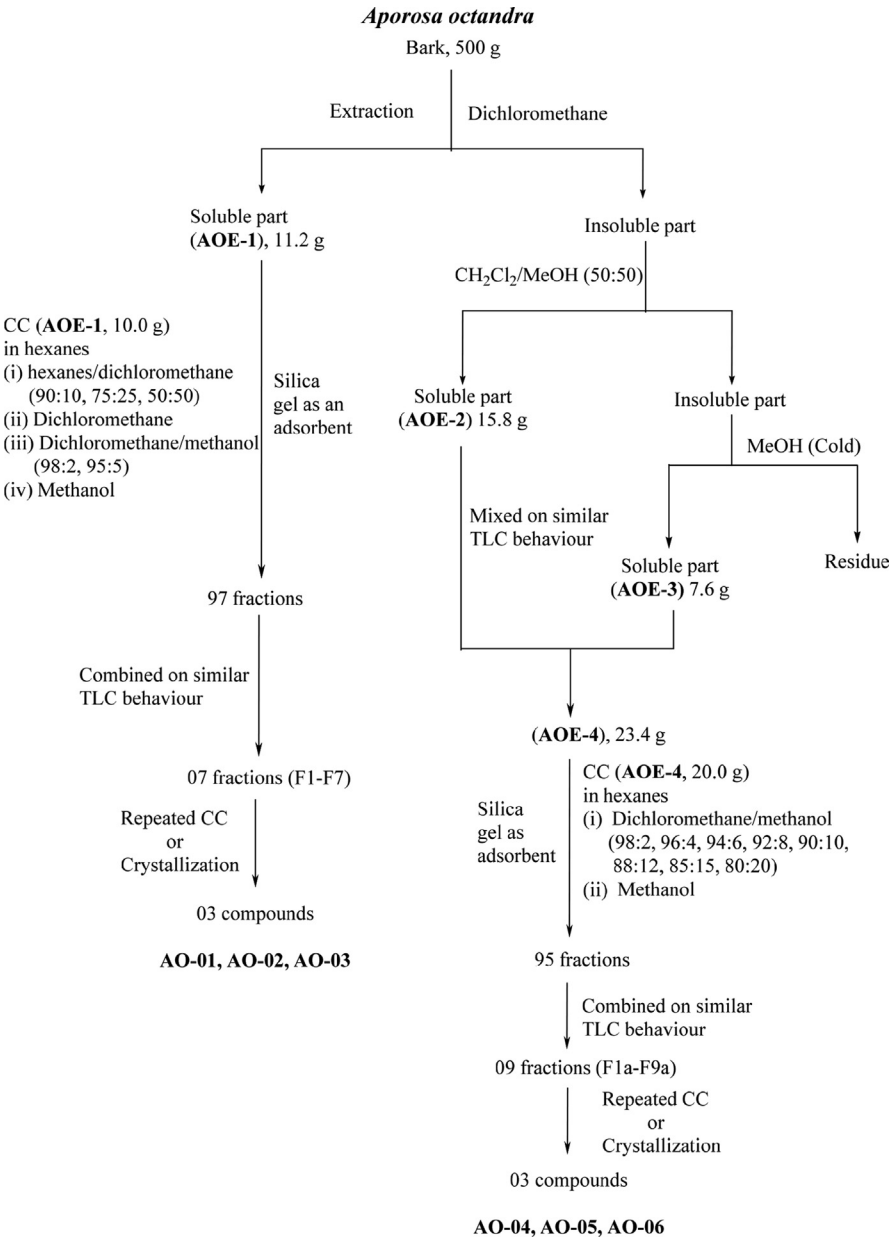

Fig. 3. Schematic representation of the extraction/fractionation process of *A.octandra*.

angle of 81.34° in addition to a hydrogen sulfide and one water molecule in the crystalline form (Fig. 5). The two atoms N11 and C12 are displaced from the plane of the heterocyclic ring N11-C10 by 0.322 Å and 0.301 Å, respectively. The overall geometrical parameters are of good agreement with previously reported structures having similar scaffolds [43, 44, 45, 46]. The principal interest in the structure lies in the inter and intra-molecular hydrogen bonds, particularly the hydrogen bonds that link the free water and hydrogen sulfide molecules with the main heterocycle (Table 6). These hydrogen bonds also stabilize the crystal structure and result in forming supramolecular layers (Fig. 6).

https://doi.org/10.1016/j.heliyon.2018.e00951

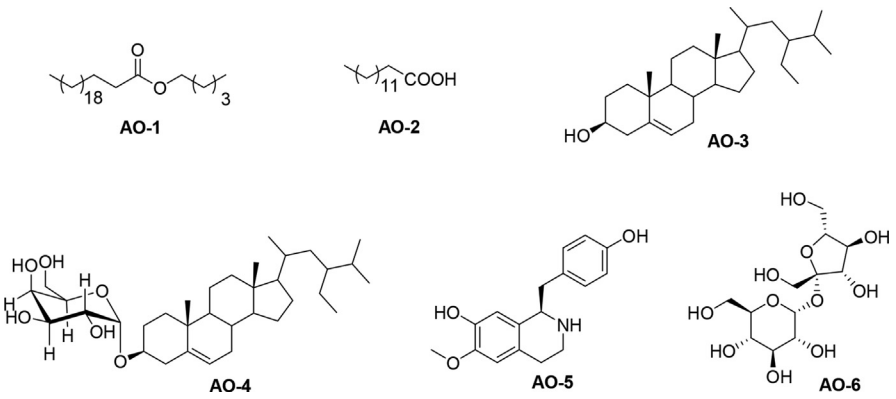

Fig. 4. Chemical structure of compounds **AO-1-AO-6** isolated from the bark of *Aporosa octandra*.

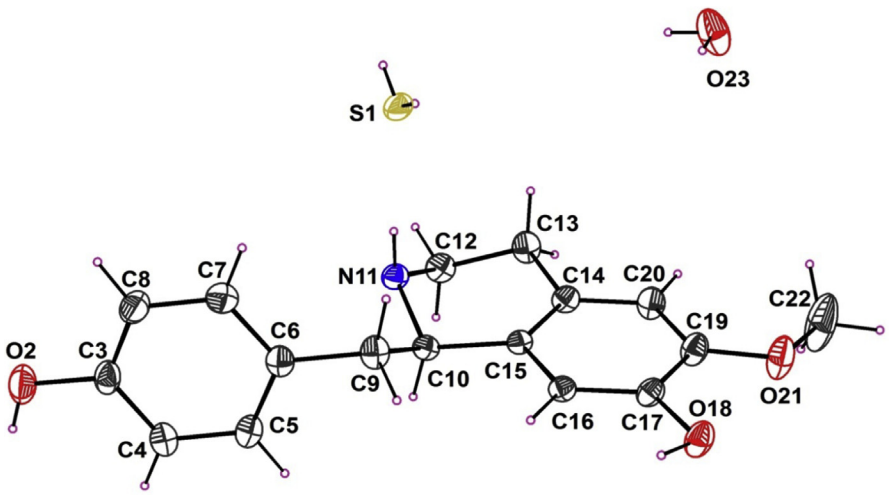

Fig. 5. ORTEP view of compound **AO-5**, showing the atom-labeling scheme. Displacement ellipsoids are drawn at the 30% probability level.

3.3. Optimized structure

Comparing the geometrical parameters of the DFT optimized structure with the experimental structure (X-ray) of **AO-5** shows a good fit (Tables 2 and 3). The highest difference between the experimental and calculated bond lengths is 0.038 Å, with root mean square error (RMSE) 0.015 Å. For bond angles, the biggest difference between the experimental and calculated values is 4.52° with RMSE 1.66°. The overall comparison was performed by superimposing the molecular skeletons obtained from X-ray diffraction with the corresponding one of the DFT method (Fig. 7). It is obvious that most functions are aligned well with each other with a little deviation. This difference is noticed for the methoxy group attached to the tetrahydroisoquinoline as the torsion angle of C20-C19-O21-C22 for the single X-ray data = −7.09°; however, for DFT it is −0.15°. This observation can be attributed to the effect of lattice form affecting the X-ray structural behavior. Whereas, in the theoretical studies this effect is completely neglected.

https://doi.org/10.1016/j.heliyon.2018.e00951

Table 6. Hydrogen-bond geometry of compound **AO-5** (Å).

D—H···*A*	*D*—H	H···*A*	*D*···*A*	*D*—H···*A*
S1—H12···N11^{i}	0.80	2.62	3.201(4)	130
O23—H231···O2^{i}	0.84	1.95	2.769(2)	164
O23—H232···O18^{ii}	0.83	2.33	3.059(2)	147
O23—H232···O21^{ii}	0.83	2.18	2.836(2)	136
O18—H181···S1^{ii}	0.85	2.32	3.158(3)	171
O2—H21···O23^{iii}	0.79	1.85	2.643(3)	176
C12—H121···S1^{iv}	0.96	2.84	3.734(2)	154

Symmetry codes: (i) 1/2+x,-1/2-y,-z; (ii) -x,-1-y,z; (iii) -1+x,y,1+z; (iv) -1+x,y,z.

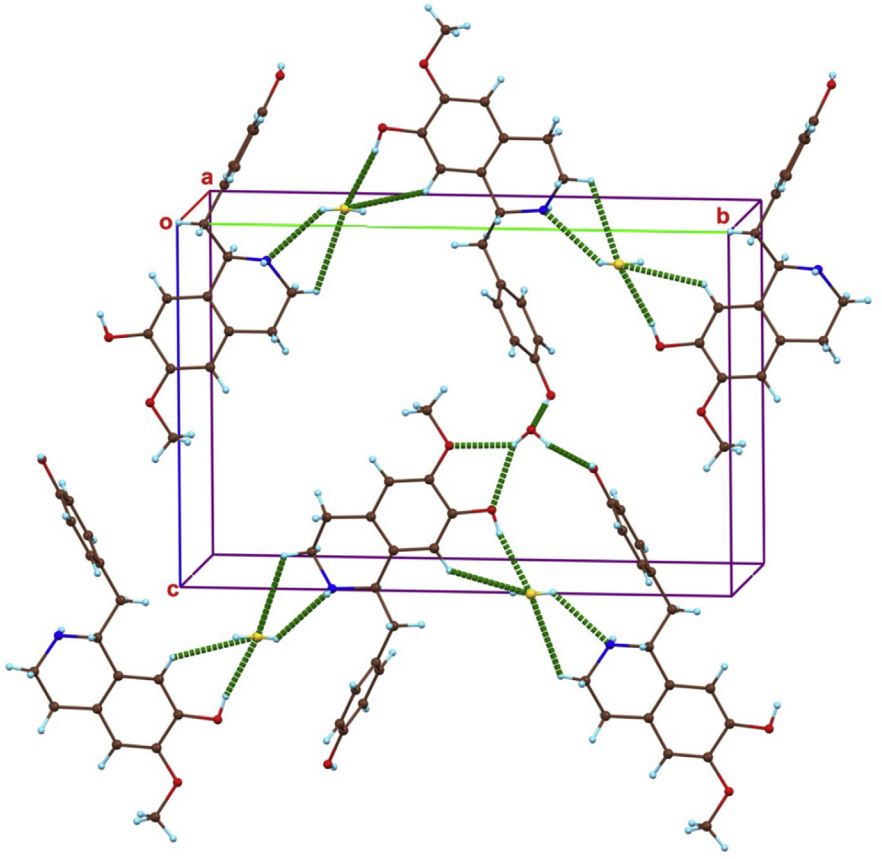

Fig. 6. Crystal packing of **AO-5** showing the hydrogen-bond interactions as dashed lines.

3.4. Computed vibrational studies

Computed IR spectrum of compound AO-5 (Table 4, Fig. 8) utilizing DFT/B3LY, 6-31G(d) basis set reveals the presence of hydroxyl and imino stretching vibration bands at $\nu = 3581, 3580\ cm^{-1}$ in addition to 2925, 2898, 2838, 1646, 1630, 1592, 1506 due to the other vibrational functions/groups. The computational

https://doi.org/10.1016/j.heliyon.2018.e00951

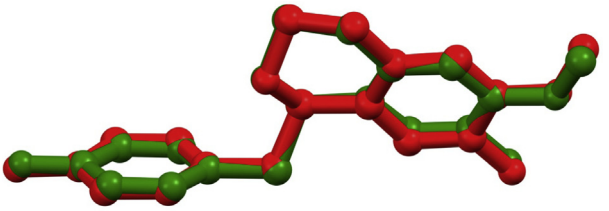

Fig. 7. Overlay diagram of compound **AO-5**, red (X-ray structure), green (DFT).

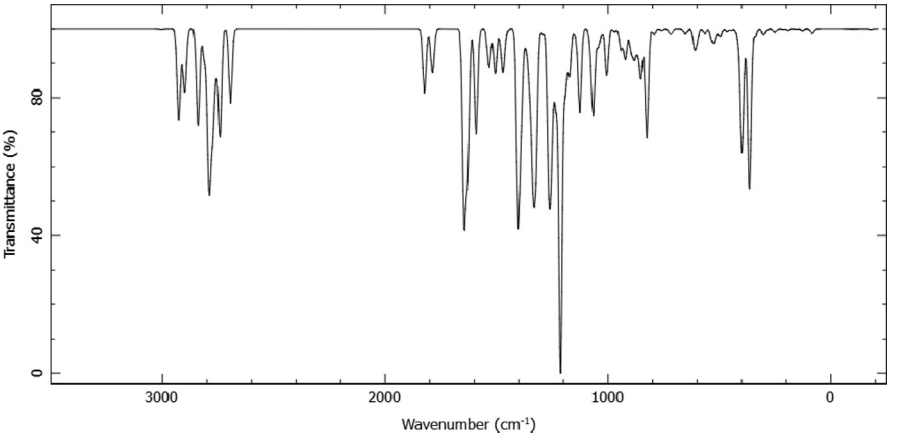

Fig. 8. Simulated IR spectrum of compound **AO-5** computed by DFT/B3LYP method with 6-31G(d) basis set.

spectrum is correlated with the experimental one considering that the difference(s) is due to the computational study is for the gaseous state while the experimental for solid state (KBr pellet).

3.5. Computed NMR studies

Theoretical ^{1}H NMR [DFT/B3LYP/6-311G+(2d,p)/GIAO] of compound **AO-5** exhibits the isoquinolinyl methylene H_2C-4 and H_2C-3 in addition to the benzylic H_2C at $\delta_H = 3.14, 3.38, 3.30$, respectively (comparable to the experimental data at $\delta_H = 3.01, 3.46, 3.33$, respectively). The isoquinolyl methine HC-1 and methoxy protons are shown at $\delta_H = 4.21, 4.25$, respectively (experimentally at $\delta_H = 4.58, 3.84$, respectively). Theoretical ^{13}C NMR reveals the isoquinolinyl C-4, C-3, C-1 and benzylic carbon at $\delta_C = 35.5, 48.8, 59.1, 46.1$, respectively (experimentally at $\delta_C = 26.0, 41.0, 57.9, 40.5$, respectively). The methoxy carbon is shown at $\delta_C = 55.0$ (experimentally at $\delta_C = 56.5$). The theoretical NMR data are derived from the gaseous state (in vacuo) but the experimental was undertaken in a solvent (MeOH-d_4). This fact can justify the difference between the experimental and computational NMR data (Table 5).

https://doi.org/10.1016/j.heliyon.2018.e00951

3.6. Biological studies

3.6.1. Effect of Aporosa octandra extract (AOE-4) on memory performance in Morris water maze experiment in D-galactose induced mice

AOE-4 (100, 200 & 300 mg/kg) per se group of animals and naive easily learned to swim straight to the platform in the Morris water maze via special navigation task on day 20. Initially, there was a sign of an increase in escape latency with the D-galactose-treated mice, which slowly declined on day 20 with continuous training through the acquisition of the navigation task. On day 20 there was significant difference in the initial acquisition latencies (IAL) value of D-galactose treated and the naive group of animals, which implies that chronic use of D-galactose impaired acquisition of spatial navigation task ($P < 0.05$). However, co-administration of D-galactose with **AOE-4** (100, 200 & 300 mg/kg) shows a significant decrease in the IAL the pre-trained animals in compared to D-galactose-treated on day 20 of the experiment (Table 7).

The mean retention latencies (1^{st} and 2^{nd} RL) and mean IAL data of the naive group and the D-galactose treated group mice on days 21 and 42 suggest D-galactose causes significant cognitive impairment in the mice [13, 14]. However, there was a significant decrease in 1^{st} RL and 2^{nd} RL on days 21 and 42, respectively in the group of mice which were administered **AOE-4** (100, 200 & 300 mg/kg) chronically to D-galactose treated mice in compared to only D-galactose treated mice (Table 7).

Table 7. Effect of *Aporosa octandra* **AOE-4** (AOE-4; 100, 200 and 300 mg/kg, p.o.) in D-galactose induced mice on memory performance in Morris water maze experiment.

Treatment (mg/kg)	Day 20 (ITL)	Day 21 (1st RTL)	Day 42 (2nd RTL)
Naïve	77.5 ± 2.4	15 ± 2.7	10.0 ± 2.5
D-Gal (100)	88 ± 2.3	87.8 ± 2.6[a]	84.3 ± 2.3[a]
AOE-4 (100)	84.5 ± 2.6	20.5 ± 2.6	18.5 ± 2.4
AOE-4 (200)	80 ± 2.5	20 ± 3	16 ± 2.1
AOE-4 (300)	79.8 ± 2.2	16.8 ± 2.7	12.5 ± 2.7
AOE-4 (100) + D-Gal (100)	83.5 ± 2.8	75.4 ± 2.5	72.8 ± 2.5
AOE-4 (200) + D-Gal (100)	78.4 ± 3	69.8 ± 2.5[b]	55.5 ± 3.2[b]
AOE-4 (300) + D-Gal (100)	75 ± 2.4	45.5 ± 2.5[b,c]	38 ± 2.4[b,c]

The initial acquisition latencies (IAL) on day 20 and retention latencies on days 21 (1^{st} RL) and 42 (2^{nd} RL) following D-gal concurrent treatment were observed. Values are mean ± S.E.M. [a]$P < 0.05$ as compared to the naive group; [b]$P < 0.05$ as compared to D-gal treated group; [c]$P < 0.05$ as compared to Aporosa (200) + D-gal group (Repeated measures one-way ANOVA followed by Tukey's test for multiple comparisons).

https://doi.org/10.1016/j.heliyon.2018.e00951

3.6.2. Effect of Aporosa octandra extract (AOE-4) on brain lipid peroxidation in D-galactose treated mice

Chronic administration of D-galactose significantly causes increase in Malondialdehyde (MDA) formation as compared to naïve mice ($P < 0.05$) [47, 48, 49]. Chronic **AOE-4** (100, 200 and 300 mg/kg, p.o.) administration significantly attenuated the oxidative damage by reducing the MDA and nitrite levels as compared to control group (D-galactose treated group) levels as well standard galantamine. Furthermore, **AOE-4** (100 mg/kg, p.o.) per se treatment did not produce any significant effect on MDA and nitrite levels as compared to naive mice (Fig. 9).

3.7. Effect of *Aporosa octandra* extract (AOE-4) on reduced glutathione, superoxide dismutase in D-galactose-treated mice

Chronic administration of D-galactose leads to significant decrease in superoxide dismutase (SOD) level in the brain as compared to naive mice ($P < 0.05$). However, chronic administration of **AOE-4** (200 and 300 mg/kg, p.o.) restores the SOD level in the D-galactose treated mice as compared to standard galantamine. Furthermore, **AOE-4** (100 mg/kg, p.o.) per se treatment did not effect on SOD levels as compared to naive mice (Fig. 10).

3.8. Effect of *Aporosa octandra* extract (AOE-4) on acetylcholinesterase activity in D-galactose treated mice

Chronic administration of D-galactose leads to significant increase in acetylcholinesterase activity as compared to naive mice ($P < 0.05$) [50]. However, chronic administration of **AOE-4** (100, 200 and 300 mg/kg, p.o.) decreases the elevated acetylcholinesterase activity in the D-galactose treated mice and the results were compared with the standard galantamine (Fig. 11).

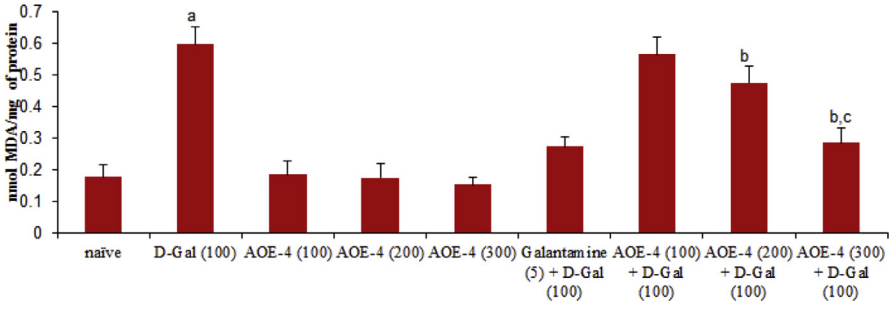

Fig. 9. Effect of *Aporosa octandra* (**AOE-4**; 100, 200 and 300 mg/kg, p.o.) on lipid peroxidation in D-galactose treated mice. Values are mean ± S.E.M. $^{a}P < 0.05$ as compared to the naïve group; $^{b}P < 0.05$ as compared to D-galactose treated group; $^{c}P < 0.05$ as compared to Aporosa (200) + D-galactose group; (Repeated measures one-way ANOVA followed by Tukey's test for multiple comparisons).

https://doi.org/10.1016/j.heliyon.2018.e00951

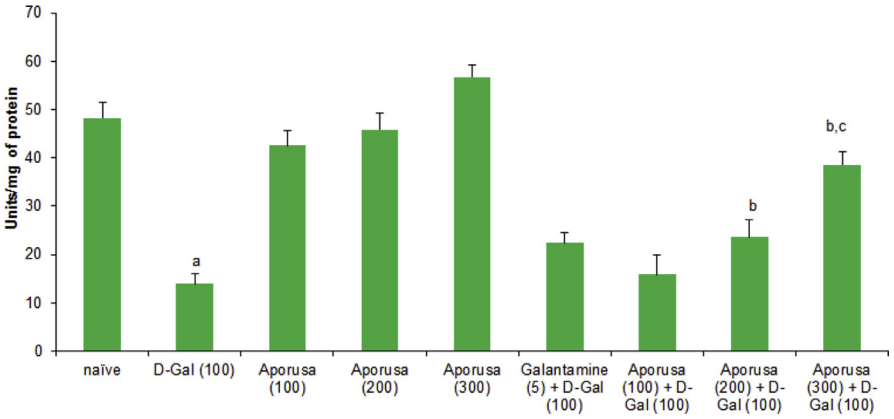

Fig. 10. Effect of *Aporosa octandra* (**AOE-4**; 100, 200 and 300 mg/kg, p.o.) on superoxide dismutase in D-galactose treated mice. Values are mean ± S.E.M. $^{a}P < 0.05$ as compared to the naïve group; $^{b}P < 0.05$ as compared to D-galactose treated group; $^{c}P < 0.05$ as compared Aporosa (200) + D-galactose group; (Repeated measures one-way ANOVA followed by Tukey's test for multiple comparisons).

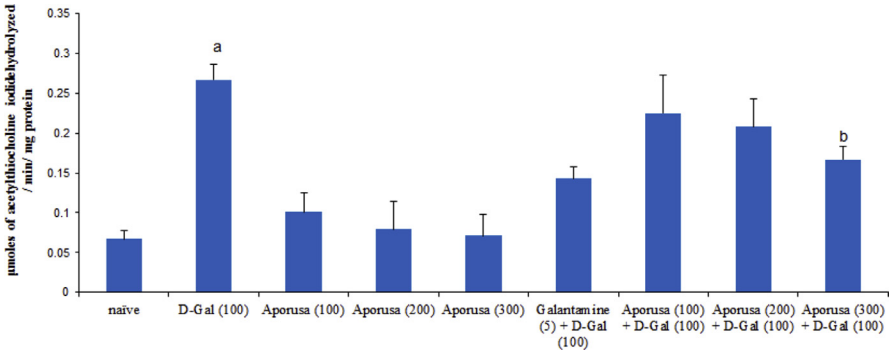

Fig. 11. Effect of *Aporosa octandra* (**AOE-4**; 100, 200 and 300 mg/kg, p.o.) on acetylcholinesterase activity in D-galactose treated mice. Values are mean ± S.E.M. $^{a}P < 0.05$ as compared to the naïve group; $^{b}P < 0.05$ as compared to D-galactose treated group; (Repeated measures one-way ANOVA followed by Tukey's test for multiple comparisons).

Several reports suggest D-galactose leads to learning & memory impairment and oxidative damage in rodents [51, 52]. Our experiments demonstrated that chronic administration of **AOE-4** extract can improve learning and memory impairment and reduced oxidative damage decreasing the elevated MDA level, restoring the reduced activity of SOD and reversed the AChE activity in D-galactose induced.

In conclusion, we identified an unexplored medicinal plant, which has the ability to control oxidative damages. To better understand the mechanism of **AOE-4** on aging and oxidative stress, further cellular level studies are required. Compound **AO-5** was characterized and is the major compound isolated from **AOE-4**. **AO-5** could be therefore used for further investigation and development of potential anti-aging agents.

https://doi.org/10.1016/j.heliyon.2018.e00951

Declarations

Author contribution statement

Siva Panda: Conceived and designed the experiments; Performed the experiments; Wrote the paper.

Subhash Jain: Conceived and designed the experiments; Contributed reagents, materials, analysis tools or data; Wrote the paper.

Atish Prakash: performed the experiments.

Adel Girgis: Analyzed and interpreted the data; Contributed reagents, materials, analysis tools or data; Wrote the paper.

Leena Khanna, Pankaj Khanna: Analyzed and interpreted the data.

ElSayed Shalaby, Nehmedo Fawzy: analyzed and interpreted the data; contributed reagents, materials, analysis tools or data.

Funding statement

This work was supported by the University of Delhi, UGC, New Delhi (number DRCH/R&D/2010−13), and Augusta University.

Competing interest statement

The authors declare no conflict of interest.

Additional information

No additional information is available for this paper.

References

[1] B.R. Troen, The biology of aging, Mt. Sinai J. Med. 70 (2003) 3−22.

[2] T.R. Golden, S. Melov, Mitochondrial DNA mutations, oxidative stress, and aging, Mech. Ageing Dev. 122 (2001) 1577−1589.

[3] N.A. Crivello, I.H. Rosenberg, G.E. Dallal, D. Bielinski, J.A. Joseph, Age-related changes in neutral sphingomyelin-specific phospholipase C activity in striatum, hippocampus, and frontal cortex: implication for sensitivity to stress and inflammation, Neurochem. Int. 47 (2005) 573−579.

[4] M.F. Beal, Aging, energy, and oxidative stress in neurodegenerative diseases, Ann. Neurol. 38 (1995) 357−366.

https://doi.org/10.1016/j.heliyon.2018.e00951

[5] P. Ulrich, A. Cerami, Protein glycation, diabetes, and aging, Recent Prog. Horm. Res. 56 (2001) 1–22.

[6] E.G. Lakatta, Arterial and cardiac aging: major shareholders in cardiovascular disease enterprises, Circulation 107 (2003) 490–497.

[7] J.-B. Zhou, Y.-L. Zheng, Y.-X. Zeng, J.-W. Wang, Z. Pei, Ji-Y. Pang, Marine derived xyloketal derivatives exhibit anti-stress and anti-aging effects through HSF pathway in Caenorhabditis elegans, Eur. J. Med. Chem. 148 (2018) 63–72.

[8] C. Kaur, H.C. Kapoor, Anti-oxidant activity and total phenolic content of some Asian vegetables, Int. J. Food Sci. Technol. 37 (2002) 153–161.

[9] Y. Cai, Q. Luo, M. Sun, H. Corke, Antioxidant activity and phenolic compounds of 112 traditional Chinese medicinal plants associated with anticancer, Life Sci. 12 (74) (2004) 2157–2184.

[10] I.M. Chang, Anti-aging and health-promoting constituents derived from traditional oriental herbal remedies: information retrieval using the TradiMed 2000 DB, Ann. N. Y. Acad. Sci. 928 (2001) 281–286.

[11] S. Bastianetto, R. Quirion, Natural extracts as possible protective agents of brain aging, Neurobiol. Aging 23 (2002) 891–897.

[12] H. Lei, B. Wang, W.P. Li, Y. Yang, A.W. Zhou, M.Z. Chen, Antiaging effect of astragalosides and its mechanism of action, Acta Pharmacol. Sin. 24 (2003) 230–234.

[13] A. Kumar, S. Dogra, A. Prakash, Effect of carvedilol on behavioral, mitochondrial dysfunction, and oxidative damage against D-galactose induced senescence in mice, Naunyn. Schmiedebergs Arch. Pharmacol. 380 (2009) 431–441.

[14] A. Kumar, A. Prakash, S. Dogra, Centella asiatica attenuates D-galactose-induced cognitive impairment, oxidative and mitochondrial dysfunction in mice, Int. J. Alzheimer's Dis. 2011 (2011).

[15] L.A. Kaplan, A.J. Pesce, Clinical Chemistry, third ed., Mosby, St. Louis, 1996, p. 954.

[16] H.M. Hsieh, W.M. Wu, M.L. Hu, Soy isoflavones attenuate oxidative stress and improve parameters related to aging and Alzheimer's disease in C57BL/6J mice treated with D-galactose, Food Chem. Toxicol. 47 (2009) 625–632.

https://doi.org/10.1016/j.heliyon.2018.e00951

[17] X. Song, M. Bao, D. Li, Y. Li, Advanced glycation in D-galactose induced mouse aging model, Mech. Ageing Dev. 108 (1999) 239–251.

[18] W.J. Baynes, The role of AGEs in aging: causation or correlation, Exp. Gerontol. 36 (2001) 1527–1537.

[19] M. Takeuchi, S. Yamagishi, Possible involvement of advanced glycation end-products (AGEs) in the pathogenesis of Alzheimer's disease, Curr. Pharmaceut. Des. 14 (2008) 973–978.

[20] Enumeration of the Flowering Plants of Nepal, vol. 3, 1982, p. 193.

[21] M.Z. Bhat, M. Ali, S.R. Mir, New flavonol diesters from the stem bark of *Ficus carica* L, Int. Res. J. Pharm. 3 (2012) 140–143.

[22] V. Theodorou, A simple method for the alkaline hydrolysis of esters, Tetrahedron Lett. 48 (2007) 8230–8233.

[23] K.S. Khetwal, Constituents of high altitude Himalayan herbs, Part III. New alkane hydroxyketones from *Tanacetum nubigenum*, J. Nat. Prod. 52 (1989) 837–839.

[24] R. Sakhuja, M. Vashist, Y.K. Bhoon, S.C. Jain, Phytochemical investigation of Tabebuia palmeri, Chem. Nat. Comp. 49 (2014) 1039–1042.

[25] A. Navarro, M.J. Sánchez Del Pino, C. Gómez, J.L. Peralta, A. Boveris, Behavioral dysfunction, brain oxidative stress, and impaired mitochondrial electron transfer in aging mice, Am. J. Physiol. Regul. Integr. Comp. Physiol. 282 (2002) R985–R992.

[26] S. Ahmad, K.K. Yadav, S.J. Singh, S.M.S. Chauhan, Synthesis of 5,10,15,20-meso-unsubstituted and 5,10,15,20-meso-substituted-21,23-ditellura/diselena core-modified porphyrinogens: oxidation and detection of mercury(II), RSC Adv. 4 (2014) 3171–3180.

[27] L. Palatinus, G. Chapuis, SUPERFLIP – a computer program for the solution of crystal structures by charge flipping in arbitrary dimensions, J. Appl. Crystallogr. 40 (2007) 786–790.

[28] P.W. Betteridge, J.R. Carruthers, R.I. Cooper, K. Prout, D.J. Watkin, CRYSTALS version 12: software for guided crystal structure analysis, J. Appl. Crystallogr. 36 (2003) 1487.

[29] R.I. Cooper, A.L. Thompson, D.J. Watkin, CRYSTALS enhancements: dealing with hydrogen atoms in refinement, J. Appl. Crystallogr. 43 (2010) 1100–1107.

https://doi.org/10.1016/j.heliyon.2018.e00951

[30] A.L. Spek, Structure validation in chemical crystallography, Acta Crystallogr. Sect. D Biol. Crystallogr. 65 (2009) 148–155.

[31] L.J. Farrugia, WinGX and ORTEP for Windows: an update, J. Appl. Crystallogr. 45 (2012) 849–854.

[32] C.F. Macrae, I.J. Bruno, J.A. Chisholm, P.R. Edgington, P. McCabe, E. Pidcock, L. Rodriguez-Monge, R. Taylor, J. van de Streek, P.A. Wood, Mercury CSD 2.0 – new features for the visualization and investigation of crystal structures, J. Appl. Crystallogr. 41 (2008) 466–470.

[33] E.M. Shalaby, A.S. Girgis, H. Farag, A.F. Mabied, A.N. Fitch, Synthesis, X-ray powder diffraction and DFT calculations of vasorelaxant active 3-(arylmethylidene)pyrrolidine-2,5-diones, RSC Adv. 6 (2016) 112950–112959.

[34] A.S. Girgis, M.N. Aziz, E.M. Shalaby, D.O. Saleh, N. Mishriky, W.I. El-Eraky, I.S.A. Farag, Molecular structure studies of novel bronchodilatory active 4-azafluorenes, Z. für Kristallogr. - Cryst. Mater. 231 (2016) 179–187.

[35] A.S. Girgis, M.N. Aziz, E.M. Shalaby, D.O. Saleh, F.M. Asaad, W.I. El-Eraky, I.S.A. Farag, Crystal structure studies and bronchodilation properties of novel benzocycloheptapyridine, J. Chem. Crystallogr. 46 (2016) 280–289.

[36] E.D. Wills, Mechanism of lipid peroxide formation in animal tissues, Biochem. J. 99 (1966) 667–676.

[37] Y. Kono, Generation of Superoxide radical during auto-oxidation of hydroxylamine and an assay for Superoxide dismutase, Arch. Biochem. Biophys. 186 (1978) 189–195.

[38] G.L. Ellman, K.D. Courtney, V. Andres Jr., R.M. Feather-Stone, A new and rapid colorimetric determination of acetylcholinesterase activity, Biochem. Pharmacol. 7 (1961) 88–95.

[39] A.G. Gornall, C.T. Bardawill, M.M. David, Determination of serum proteins by means of Biuret reaction, J. Biol. Chem. 177 (1949) 751–766.

[40] Y. Kashiwada, A. Aoshima, Y. Ikeshiro, Y.-P. Chen, H. Furukawa, M. Itoigawa, T. Fujioka, K. Mihashi, L.M. Cosentino, S.L. Morris-Natschke, Anti-HIV benzylisoquinoline alkaloids and flavonoids from the leaves of Nelumbo nucifera, and structure-activity correlations with related alkaloids, Bioorg. Med. Chem. 13 (2004) 443–448.

[41] Y. Nishiyama, M. Moriyasu, M. Ichimaru, K. Iwasa, A. Kato, S.G. Mathenge, P.B. Chalo Mutiso, F.D. Juma, Secondary and tertiary isoquinoline alkaloids from Xylopia parviflora, Phytochemistry 67 (2006) 2671–2675.

 https://doi.org/10.1016/j.heliyon.2018.e00951

[42] M.s B. Machado, L.M.X. Lopes, Dimeric alkaloids and flavonoids from Aristolochia ridicula, Biochem. Syst. Ecol. 38 (2010) 110–115.

[43] A. Lehmann, L. Lechner, K. Radacki, H. Braunschweig, U. Holzgrabe, Crystal structure of (3S*,4R*)-4-fluoro-3-(4-methoxyphenyl)-1-oxo-2-phenyl-1,2,3,4-tetrahydroisoquinoline-4-carboxylic acid, Acta Crystallogr. E73 (2017) 867–870.

[44] T. Naicker, T. Govender, H.G. Kruger, G.E.M. Maguire, Optically active diaryl tetrahydroisoquinoline derivatives, Acta Crystallogr. C67 (2011) o100–o103.

[45] A. Subbiah Pandi, V. Rajakannan, D. Velmurugan, M. Parvez, M.-J. Kim, A. Senthilvelan, S. Narasinga Rao, Three tetrahydroisoquinolinedione derivatives, Acta Crystallogr. C58 (2002) o164–o0167.

[46] K.K. Turgunov, Sh.N. Zhurakulov, U. Englert, V.I. Vinogradova, B. Tashkhodjaev, Synthesis of 2-(2-hydroxyethyl)-1-(2-hydroxyphenyl)-6,7-dimethoxy-1,2,3,4-tetrahydroisoquinoline and pseudosymmetry in its crystal structure, Acta Crystallogr. C72 (2016) 607–611.

[47] X. Cui, Z. Pingping, Z. Qing, L. Xuekun, H. Yazhuo, L. Jiangang, P. Lester, L. Jiankang, Chronic systemic D-galactose exposure induces memory loss, neurodegeneration, and oxidative damage in mice: protective effects of R-a-lipoic acid, J. Neurosci. Res. 84 (2006) 647–654.

[48] S.-C. Ho, L. Jue-Hao, W. ReY-Yih, Establishment of the mimetic aging effect in mice caused by D-galactose, Biogerontology 4 (2003) 15–18.

[49] Y.X. Shen, S.Y. Xu, W. Wei, X.X. Sun, J. Yang, L.H. Liu, C. Dong, Melatonin reduces memory changes and neural oxidative damage in mice treated with D-galactose, J. Pineal Res. 32 (2002) 173–178.

[50] S.-Z. Zhong, G. Qing-Hua, Q. Rong, L. Qiao, M. Shi-Ping, Paeonol attenuates neurotoxicity and ameliorates cognitive impairment induced by D-galactose in ICR mice, J. Neurol. Sci. 277 (2009) 58–64.

[51] Y.Z. Shang, M.Y. Gong, X.X. Zhou, S.T. Li, B.Y. Wang, Improving effects of SSF on memory deficits and pathological changes of neural and immunological systems in senescent mice, Acta Pharmacol. Sin. 22 (2001) 1078–1083.

[52] H. Wei, L. Lin, S. Qiujie, A. Houxi, C. Jin, L. Wei, Behavioural study of the D-galactose induced aging model in C57BL/6J mice, Behav. Brain Res. 157 (2005) 245–251.

https://doi.org/10.1016/j.heliyon.2018.e00951